Open access • Journal Article • DOI:10.1063/1.449693

The drainage of thin liquid films between solid surfaces — Source link

Derek Y. C. Chan, Roger G. Horn

Published on: 01 Jan 1985 - Journal of Chemical Physics (American Institute of Physics)

Topics: Thin film and Lubrication

The drainage of thin liquid films between solid surfaces

D. Y. C. Chan[a] and R. G. Horn
Department of Applied Mathematics, Research School of Physical Sciences, Australian National University, Canberra 2600, Australia

(Received 2 May 1985; accepted 3 June 1985)

We present measurements of the thickness as a function of time of liquid films as they are squeezed between molecularly smooth mica surfaces. Three Newtonian, nonpolar liquids have been studied: octamethylcyclotetrasiloxane, *n*-tetradecane, and *n*-hexadecane. The film thicknesses are determined with an accuracy of 0.2 nm as they drain from $\sim 1\,\mu$m to a few molecular layers. Results are in excellent agreement with the Reynolds theory of lubrication for film thicknesses above 50 nm. For thinner films the drainage is slower than the theoretical prediction, which can be accounted for by assuming that the liquid within about two molecular layers of each solid surface does not undergo shear. In very thin films the continuum Reynolds theory breaks down, as drainage occurs in a series of abrupt steps whose size matches the thickness of molecular layers in the liquid. The presence of trace amounts of water has a dramatic effect on the drainage of a nonpolar liquid between hydrophilic surfaces, causing film rupture which is not observed in the dry liquids.

I. INTRODUCTION

It is almost 100 years since Reynolds[1] published his analysis of hydrodynamic lubrication due to a thin macroscopic film of liquid confined between two moving solid surfaces. This theory is based on a simplification of the Navier–Stokes equations of continuum hydrodynamics by exploiting the special geometry of thin films. The utility of this theory still stands today and many extensions and applications of the original analysis may be found in text books on hydrodynamic lubrication theory.[2]

Apart from obvious engineering applications, the Reynolds theory has also been used to explain the rate of drainage of thin films of liquid between solid, liquid, or vapor surfaces (for reviews see Refs. 3–5). This is an important factor in determining the coagulation of colloids, the coalescence of liquid emulsions, and the collapse of foams. A corollary of this is the use of measurements of the drainage rate to obtain information on the surface forces, e.g., van der Waals and electrical double layer forces, which drive the drainage of thin films. By *assuming* that the hydrodynamic behavior of the system is adequately described by the Reynolds theory it is possible to deduce the form of the surface forces from the time dependence of the drainage process. The early work in this area, initiated by Derjaguin and co-workers, and by Scheludko and co-workers, has appeared in a number of reviews.[6–8] Hough and Ottewill have recently used a similar method to deduce the surface forces from the drainage of the liquid film between a rubber sphere and a glass plate.[9]

In this paper we introduce a method of measuring the time evolution of the drainage of a liquid film between two molecularly smooth mica surfaces. It is based on the apparatus developed by Israelachvili[10] which has hitherto been used to make static measurements of surface forces, and has the ability to measure film thicknesses from a few μm down to zero with a resolution of ~ 0.1 nm. We therefore have a near-ideal experiment in which to test the Reynolds theory of drainage right down to the thinnest films.

Surface force measurements made with this apparatus have shown that continuum theories of van der Waals and electrical double layer forces are no longer valid for very thin films,[11–13] where it becomes necessary to take into account the molecular nature of the intervening liquid. In particular, the monotonic separation dependence of these surface forces becomes an oscillatory function of separation, and the period of the oscillations matches the molecular size of the liquids. The exact separation at which these forces become oscillatory depends on the properties of the liquid as well as that of the surfaces. These deviations from the predictions of continuum theory are referred to as solvation effects and the oscillatory forces as solvation forces.

In previous studies of the drainage of thin films the hydrodynamics has always been described by the macroscopic continuum Navier–Stokes equations or the Reynolds theory. Thus the question arises as to the limits in which hydrodynamic equations can be applied. Clearly for sufficiently thin films the concept of a continuum liquid with a well defined viscosity must become inappropriate. The present work is the first attempt to address this and other related questions.

As an initial application of the experimental technique (Sec. II) and the theoretical background needed to analyze the experiments (Sec. III and Appendices), we have chosen to study three simple, nonpolar, Newtonian liquids: octamethylcyclotetrasiloxane (OMCTS), *n*-tetradecane, and *n*-hexadecane. In a parallel study, Israelachvili has used the same apparatus and a slightly different technique to measure the viscosities of *n*-tetradecane and aqueous electrolyte solutions in thin films.[14] Extensions of either method to study other liquids would be straightforward.

For the liquids we have considered, the only surface forces present are relatively weak and short-ranged van der Waals and solvation forces. Our results, presented in Sec. IV and discussed in Sec. V, show that in such cases the Reynolds

[a] Present address: Department of Mathematics, University of Melbourne, Parkville, Victoria 3052, Australia

description of the drainage process appears to be very accurate down to film thickness of about 50 nm, and no departure from the bulk value of the liquid viscosity is detected. For thinner films (down to about 5 nm) the observed rate of film drainage is slightly *slower* than that predicted by theory. This discrepancy can be accounted for empirically by the assumption that very thin regions of the liquid near the mica surfaces do not undergo shear. We emphasize that our results do not *prove* the existence of such immobile layers of liquid; this is merely a simple-minded yet convenient parametrization to account for experimental observations. Finally, when the film is less than about ten molecules thick, the continuum model breaks down. A description of the drainage of such thin films must await a microscopic model for the flow behavior of a collection of molecules near a solid boundary.

II. THE EXPERIMENT

We have used the surface forces apparatus developed by Israelachvili,[10] to measure the drainage of liquid films on a very fine scale. In this apparatus, illustrated schematically in Fig. 1, two thin sheets of molecularly smooth mica are glued to cylindrical lenses of fused silica. The lenses are mounted with the mica sheets facing each other and the cylindrical axes at right angles, so that they meet at a point. If the radii of the cylinders are equal and their separation is much less than the radius R, the distance between the surfaces is equivalent to that between a sphere and a flat plate. Typically we have $R \gtrsim 1$ cm and $D \lesssim 1\ \mu$m, so $D/R \lesssim 10^{-4}$ throughout our experiment.

The minimum separation between the mica sheets is measured by an optical interference technique. A silver coating of reflectivity $\gtrsim 95\%$ is applied to the outside of each mica sheet, i.e., the side adjacent to the silica lens. When white light enters the system, only certain wavelengths, which satisfy an interference condition depending on the optical thickness between the silver layers, are transmitted. A spectrometer splits the transmitted light into its component wavelengths, and *fringes of equal chromatic order*[15] are viewed at the spectrometer exit. Measurements of fringe wavelength allow the separation D to be computed, where $D = 0$ refers to the mica surfaces in molecular contact, which is established by bringing the surfaces together in a nitrogen atmosphere before filling the apparatus with liquid. The observed fringes are extremely sharp because of multiple reflections and the exceptional smoothness of the silver layers deposited on mica, and in practice it is possible to measure D with a resolution of 0.1 nm.

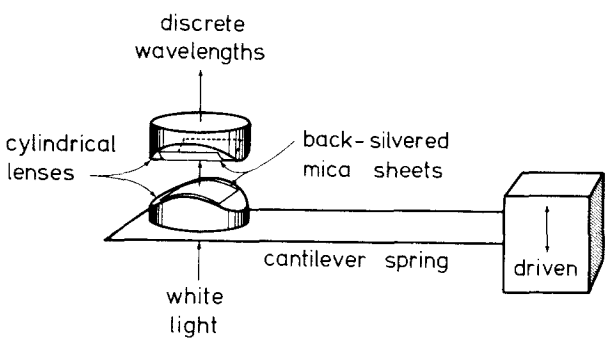

FIG. 1. Schematic diagram of the experimental arrangement. Optical interference "fringes of equal chromatic order" (Ref. 15) are used to measure the separation between two mica sheets glued to crossed cylinders of silica. The end of the cantilever spring remote from the lens can be moved up or down at a constant speed, or (equivalently) held fixed while the upper lens is moved using a piezoelectric transducer. For further details see Ref. 10.

For the dynamic measurements required here, we have used a video camera at the spectrometer exit to film the movement of the fringes, together with a clock recording. The wavelength at any instant can subsequently be measured from the video recording using a Video Micrometer (Colorado Video Inc. model 305), and thus the separation $D(t)$ can be computed as a function of time. Separations measured in this way have a slightly larger error, about ± 0.2 nm for the results presented in Sec. IV.

As shown in Fig. 1, one of the mica-covered lenses is mounted on a cantilever spring, whose deflection is used to measure the force exerted on that mica surface as it approaches the other. The cantilever spring and both surfaces are immersed in the liquid being studied. The end of the spring away from the lens can be moved at a constant speed relative to the other lens, either by a synchronous motor driving a micrometer whose motion is reduced by a differential-spring mechanism, or by a piezoelectric ceramic transducer. However, the progressive deflection of the spring due to hydrodynamic and surface forces means that the lens itself does not move at a constant speed. The equation describing its motion is discussed below.

Experiments were carried out on three organic liquids: octamethylcyclotetrasiloxane (OMCTS), *n*-tetradecane, and *n*-hexadecane. The first was obtained from Fluka, Purum grade, and the other two from Sigma (99%). All liquids were distilled twice under N_2 at reduced pressure. Some P_2O_5 was placed in the experimental apparatus to scavenge any water dissolved in the liquids, because even trace amounts of water have been found to have a dramatic effect on the equilibrium force between mica sheets in organic liquids.[11,12,16] In one experiment, discussed in Sec. IV D, the P_2O_5 was removed to see how the presence of water affects the drainage of OMCTS.

III. THE EQUATION OF MOTION

For the sake of brevity only a condensed description of the theory is given here, most of the detail being relegated to the Appendices.

In Appendix A, we calculate the hydrodynamic force F_H between crossed cylinders of radii R_1 and R_2 immersed in a liquid of viscosity η, with stick boundary conditions at the cylindrical surfaces. If the cylinders are separated by a distance D and one of them is moving along a line normal to both surfaces, the other experiences a force [Eq. (A16)]:

$$F_H = -\frac{6\pi\eta R_H R_G}{D}\frac{dD}{dt}. \tag{3.1}$$

Here $R_H = [\frac{1}{2}(1/R_1 + 1/R_2)]^{-1}$ is the harmonic mean and $R_G = (R_1 R_2)^{1/2}$ is the geometric mean of the cylinder radii. Positive values of F_H correspond to repulsion. For R_1

$= R_2 = R$, $F_H = -(6\pi\eta R^2/D)(dD/dt)$, which has the appearance of a Stokes drag on a sphere [$(6\pi\eta R)\times$ velocity], amplified by a geometric factor (R/D).

A simple force balance between the surfaces gives

$$F_H + F_S = F_K, \tag{3.2}$$

where F_S is the surface force and F_K the restoring force of the cantilever spring. This can be written as

$$-\frac{6\pi\eta R_H R_G}{D(t)}\frac{dD}{dt} + (2\pi R_G) E_P(D(t)) = K\Delta(t). \tag{3.3}$$

Although the expression for the hydrodynamic force is strictly only valid when the relative velocity of the surfaces dD/dt is constant, for a sufficiently slow approach this pseudo-steady approximation will suffice. The second term in Eq. (3.3) is the Derjaguin[17] expression for the surface force F_S between crossed cylinders with $E_P(D)$ being the interaction free energy per unit area between parallel planes. This expression for the surface force is valid for $R_G \gg D$ which is the regime of experimental interest in this paper. In this connection it is interesting to observe that in all previous applications of the drainage method to measure surface forces, the surfaces were always assumed to be parallel planes so the force between the surfaces had the form $\pi R^2 F_P(D)$ where $F_P(D)$ is the *force* per unit area between flat surfaces and πR^2 is the *constant* area of contact. For drainage under nonretarded van der Waals interactions the parallel plane approximation would predict that $D(t)$ is proportional to $(t_c - t)$, whereas the use of curved surfaces and the Derjaguin approximation would predict that $D(t)$ is proportional to $(t_c - t)^{1/2}$, where t_c is the time at which the surfaces come into contact, $D(t_c) = 0$ [cf. Eq. (3.12)]. Indeed the use of the parallel plane approximation may lead to an erroneous form for the deduced interaction if the surfaces are not strictly flat.

We have assumed that any surface forces present are unaffected by the relative motion of the surfaces and are thus taken to be the equilibrium forces. This is valid provided the relative velocity is sufficiently slow compared to the characteristic relaxation times of the mechanisms that give rise to the surface forces. For instance, when steric interactions are present the relatively long time required for the rearrangement of macromolecules may give rise to velocity dependent visco-elastic effects which are not present in equilibrium force measurements.

The right-hand side of Eq. (3.3) is the restoring force due to the spring, F_K, which is proportional to the instantaneous deflection $\Delta(t)$ of the spring from its equilibrium position multiplied by the spring constant K. We take $\Delta > 0$ when the spring is bent outward by a repulsion between the surfaces, as shown schematically in Fig. 2.

In writing down Eqs. (3.2) and (3.3) we have ignored inertial or acceleration effects. A simple calculation indicates that acceleration effects are smaller than one part in 10^4 in comparison with the hydrodynamic force. That is, the system is strongly overdamped. We have also omitted separation-independent Stokes type frictional drag forces. The magnitude of such forces would be of the order $6\pi\eta R\,(dD/dt)$ which is smaller than the hydrodynamic force due to lubrication effects by a factor $(D/R) \lesssim 10^{-4}$.

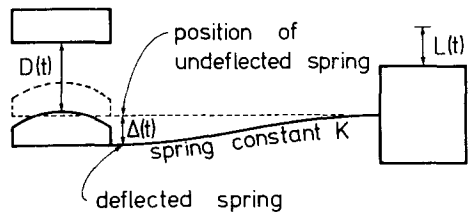

FIG. 2. Deflection of the cantilever spring by a distance Δ when there is a hydrodynamic and/or surface force between the two mica sheets.

We note from Eq. (3.3) that the hydrodynamic force increases as the product $R_H R_G$, while the surface force is linear in R_G. Thus the relative importance of the three terms in Eq. (3.3) can be controlled by suitable adjustment of the spring constant and the cylinder radii.

To complete the description of the system, we have the geometric constraint (see Fig. 2), valid at all times t,

$$L(t) + \Delta(t) - D(t) = L(0) + \Delta(0) - D(0), \tag{3.4}$$

where $L(t)$ is the displacement of the end of the spring relative to some arbitrary datum. Without loss of generality we choose the constant $L(0) + \Delta(0) - D(0)$ to be zero, so that

$$\Delta(t) = D(t) - L(t). \tag{3.5}$$

From Eq. (3.3) we see that the initial spring deflection is

$$\Delta(0) = \frac{-6\pi\eta R_H R_G}{K}\frac{1}{D(0)}\frac{dD}{dt}\bigg|_{t=0} + \frac{2\pi R_G}{K}E_P(D(0)). \tag{3.6}$$

The driving function $L(t)$ could be any single-valued function, for example sinusoidal.[14] However, in the experiments reported here we have restricted ourselves to constant velocity drives, so $L(t)$ has the form

$$L(t) = L(0) + Vt = D(0) - \Delta(0) + Vt, \tag{3.7}$$

where V is the driving speed. We choose $V < 0$ when the surfaces are being driven towards each other.

Figure 3 illustrates various types of driving function that have been employed in our experiment, and the corresponding response of the surface separation $D(t)$. For most of the data presented below, the initial separation $D(0) \gtrsim 200$ nm, whereas the surface forces acting (van der Waals and solvation forces) are negligible for separations $D \gtrsim 20$ nm. (Electrical double layer forces could be of longer range, but they are immeasurably small in the nonpolar liquids studied here). Hence, there is a considerable distance regime in which the surface force term may be omitted from Eq. (3.3). Under these conditions, solutions to the equation of motion can be derived for the various types of driving function. This is done in Appendix B.

When a surface force term is included in Eq. (3.3), it is no longer possible, in general, to obtain a solution in closed form. The equation is then solved numerically using a fourth-order Runge–Kutta method to calculate $D(t)$ for a given surface force $F_S(D)$. In the nonpolar liquids studied here, the only force acting at large separations is the continuum van der Waals attraction

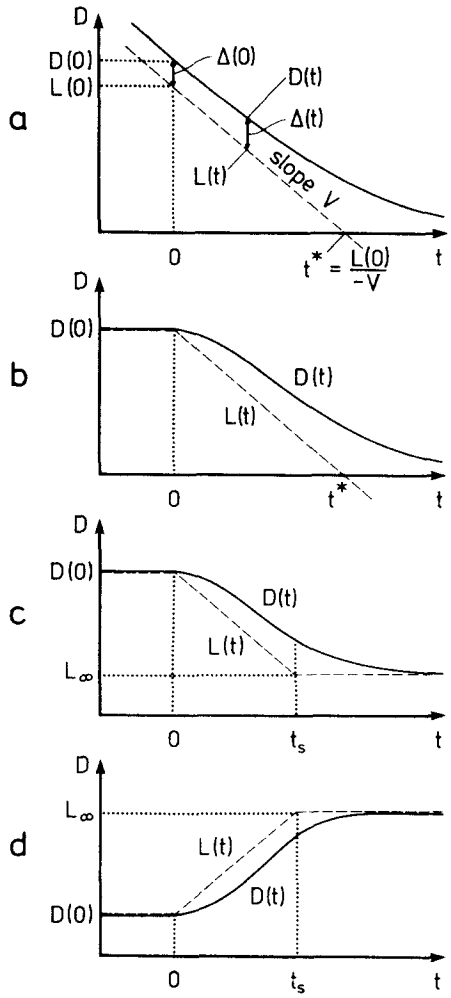

FIG. 3. Illustration of the various types of movement employed in these experiments. In each case the dashed line shows the drive function $L(t)$ and the solid curve the response of one surface with respect to the other. (a) *Flying start.* The spring is driven at a constant speed $V<0$ (surfaces approaching), starting at a time $t<0$. The spring deflection at time zero, $\Delta(0)$, is given by Eq. (3.6). If the spring were infinitely rigid the surfaces would come into contact ($D=0$) at time $t^*=L(0)/(-V)$. (b) *Standing start.* Spring driven at constant speed $V<0$, starting from rest at $t\leqslant 0$. (c) *Limited-time run, inwards.* The spring is driven inwards during the interval $0<t<t_s$, and is held stationary otherwise. $L_\infty = D(0) + Vt_s$ is the final position of the spring. (d) *Limited-time run, outwards.* As for (c), except that the speed $V>0$, i.e., the surfaces are driven apart.

$$F_{\mathrm{vdW}} = -\frac{R_G A}{6D^2}, \tag{3.8}$$

where A is the Hamaker constant. At small separations, the interaction becomes an oscillatory function of the separation. For the purpose of this study we *model* this oscillatory effect as an additional term

$$F_{\mathrm{solv}} = -R_G\, B e^{-D/\xi_1} \cos(2\pi D/\xi_2) \tag{3.9}$$

in which the parameters B, ξ_1, ξ_2 are obtained by fitting to equilibrium force measurements. Thus we set

$$F_S = F_{\mathrm{solv}} + F_{\mathrm{vdW}} = -R_G\left[\frac{A}{6D^2} + Be^{-D/\xi_1}\cos\left(\frac{2\pi D}{\xi_2}\right)\right] \tag{3.10}$$

as an *empirical* form of the surface force, which can readily be incorporated in the numerical routine to compute the drainage curve $D(t)$.

In passing, we note that in the absence of surface forces the solution [Eq. (B11)] predicts that $D(t)\to 0$ only asymptotically in the limit $t\to\infty$, because the viscous drag $F_H(D) \sim 1/D$. However, with an attractive van der Waals force of the form (3.8), the surfaces come into contact ($D=0$) at a finite time. At sufficiently small separations we can neglect the right-hand side of Eq. (3.3) since the restoring force of the spring becomes much smaller than the other terms $F_H \sim 1/D$ and $F_S \sim 1/D^2$. The equation becomes

$$\frac{6\pi\eta R_H R_G}{D(t)}\frac{dD(t)}{dt} + \frac{R_G A}{6D^2(t)} = 0 \tag{3.11}$$

which has the solution

$$D(t) = \left[\frac{A}{18\pi\eta R_H}(t_c - t)\right]^{1/2}, \tag{3.12}$$

t_c being the time at which the surfaces come into contact, $D(t_c)=0$.

IV. RESULTS

A. Octamethylcyclotetrasiloxane (OMCTS)

This liquid, a low molecular weight relative of the silicone oils, has previously been studied in equilibrium surface force measurements.[11,12,18] As discussed above, the results show an oscillatory function of distance with a periodicity approximately equal to the molecular diameter $\sigma \approx 0.8$ nm. The magnitude of the force has been found to be rather variable from one experiment to another, depending on trace amounts of impurities at the mica-liquid interface. For this reason static measurements of the surface force were made in the same experiment as the dynamic measurement, i.e., using the same mica sheets and liquid sample. Figure 4 shows the results, together with an empirical force law of the form

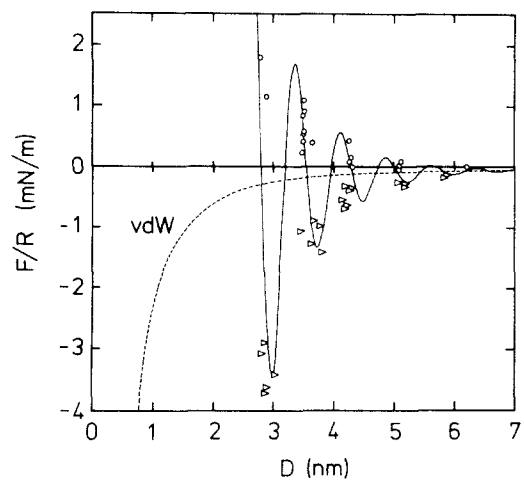

FIG. 4. The equilibrium surface force between two mica sheets in OMCTS, measured in the same experiment as the drainage results of Figs. 5–7. Open circles are measurements made along those parts of the force curves having negative slope; arrowheads indicate points measured at force minima (Ref. 11). The continuous curve is an approximate empirical fit of the form (3.10), $F/R\,(\mathrm{mN/m}) = -[14/6D^2 + 172e^{-D/0.75}\cos(2\pi D/0.75)]$ (D in nm); the dashed curve shows the continuum van der Waals attraction alone.

(3.10) with the parameters $A = 1.4\times10^{-20}$ J,[11] $B = 172$ mN/m, and $\xi_1 = \xi_2 = 0.75$ nm. This is not a perfect description of the measured force, but it is adequate for the present purpose of computing the theoretical drainage curve.

To compare our experimental results for the dynamic approach of the mica surfaces in OMCTS with the theoretical prediction, we also need to know the value of the experimental constant

$$\alpha = \frac{6\pi\eta R_H R_G}{K}. \tag{4.1}$$

In principle all of the quantities η, K, and $R_H R_G = 2(R_1 R_2)^{3/2}/(R_1 + R_2)$, where R_1 and R_2 are the radii of the two mica cylinders, are known: the spring constant K is calibrated by measuring the deflection when small weights are placed on the spring, R_1 and R_2 are determined from the shape of the fringes of equal chromatic order viewed in the spectrometer, and we use a literature value for η. In practice, however, there are errors in each of these measurements, estimated as 5% in K, 5% in each of R_1 and R_2, and 1% in η (arising chiefly from the uncertainty in temperature), which compound to an uncertainty of $\sim$20% in the value of α.

Alternatively, the value of α appropriate for a particular experiment could be established directly by the method suggested in Appendix B 3. There it is shown that for a "limited-time" run [Fig. 3(c)] in the regime $D \gtrsim 20$ nm where surface forces can be neglected, the surface separation measured after the drive is stopped at time t_s obeys the equation

$$\frac{D(t) - L_\infty}{D(t)} = \left[\frac{D(t_s) - L_\infty}{D(t_s)}\right] \exp\left\{-\frac{L_\infty}{\alpha}(t - t_s)\right\}, \tag{4.2}$$

where $L_\infty = D(0) + Vt_s$ is the final value of the driving function. Thus a plot of $\ln\{[D(t) - L_\infty]/D(t)\}$ against $(t - t_s)$ should give a straight line with decay time α/L_∞.

Figure 5 shows results plotted in this way, for a set of runs in which the mica surfaces were driven towards each other using the piezoelectric ceramic transducer (at $V = -23.4$ nm/s for $t_s = 5$ s), starting at various separations from $D(0) \approx 1000$ down to 100 nm. The data are well fitted by stright lines, and the decay times for each case give a value $\alpha = (5.4 \pm 0.1)\times10^{-7}$ m s (Table I). No systematic variation of α is observed, which indicates that the viscosity η does not depart measurably from its bulk value, at least down to a few tens of nm.

The experimental constant established in this way is to be compared with the value calculated from the measured values $R_1 = (2.2 \pm 0.1)$ cm, $R_2 = (4.3 \pm 0.2)$ cm, $K = (86 \pm 4)$N/m, and $\eta = (2.35 \pm 0.02)$ cP[19] for the temperature 21.5 ± 0.3 °C at which this experiment was carried out. These data give $\alpha = (4.6 \pm 1.0)\times10^{-7}$ m s, a range which includes the above value. Clearly, however, the use of Eq. (4.2) gives a more accurate determination, and in what follows the value $\alpha = 5.4\times10^{-7}$ m s is used to compute all the theoretical curves appropriate for this experiment.

The complete limited-time piezoelectric transducer-driven drainage runs $D(t)$ are shown in Fig. 6. Having established the value of α by the procedure described above, which uses only those data obtained *after* the drive was stopped, and knowing the driving speed $V = [L_\infty - D(0)]/t_s$, there are no further adjustable parameters used to generate the entire set of theoretical curves. The agreement with experiment is extremely good throughout, though not quite perfect at small separations. This region is examined in more detail below.

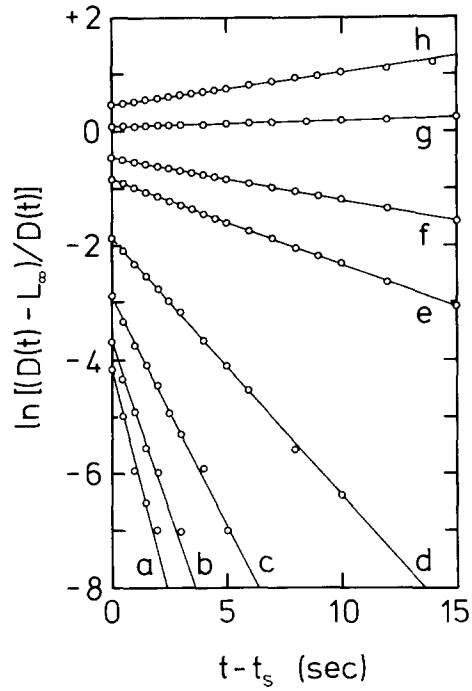

FIG. 5. Data (open circles) obtained from limited-time drainage runs in OMCTS, after the driven is stopped at $t = t_s$. Equation (4.2) predicts that the function $\ln\{[D(t) - L_\infty]/D(t)\}$ should decay exponentially in this regime, with decay time α/L_∞, where α is the experimental constant $6\pi\eta R_G R_H/K$. The different lines were measured at different separations (see Fig. 6), line (a) being at the largest separation and having the shortest decay time. The values of L_∞, decay time and α for each line are given in Table I.

The alternative method of driving the surfaces using a constant speed motor was not so successful for limited-time runs, because of small but measurable imperfections in the drive function $L(t)$ when the motor is started and stopped. However, the motor does have the advantage of a much larger range in $L(t)$, and so could be used to generate the types of

TABLE I. Values of the final drive position L_∞, the decay time α/L_∞, and hence the derived value of the experimental constant $\alpha = 6\pi\eta R_G R_H/K$, for each of the lines shown in Fig. 5.

Line	L_∞ (nm)	Decay time (s)	α ($\times10^{-7}$ m s)
a	874.8	0.63	5.5
b	668.1	0.82	5.5
c	439.5	1.22	5.36
d	238.1	2.25	5.36
e	79.1	6.70	5.30
f	39.5	13.5	5.33
g	− 6.4	− 84	5.4
h	− 32.5	− 17	5.5
			5.4 ± 0.1

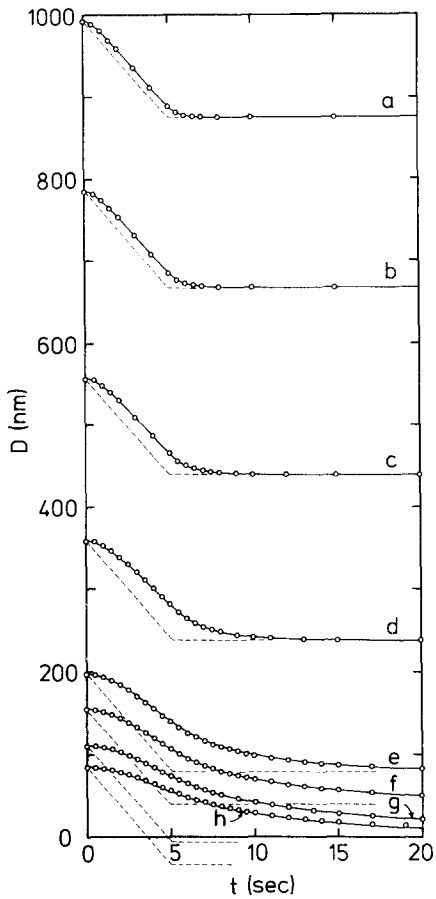

FIG. 6. A set of limited-time drainage runs in OMCTS, in which the surfaces were driven towards each other for 5 s at $V = -23.4$ nm/s. Labels a–h correspond to the lines shown in Fig. 5, which were derived from these data for $t \geqslant 5$ s. Dashed lines show the drive functions; continuous curves show the response $D(t)$ predicted by the Reynolds drainage theory with the experimental constant $\alpha = 5.4 \times 10^{-7}$ m s (Table I). The excellent agreement indicates that the viscosity (incorporated in α) maintains its bulk value right down to very thin liquid films.

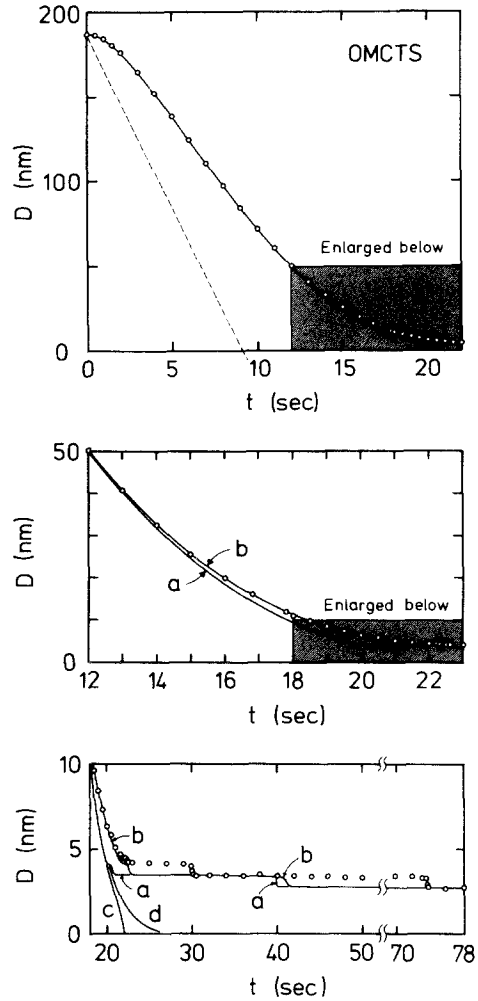

FIG. 7. Results of a standing start drainage run in the same OMCTS experiment with $\alpha = 5.4 \times 10^{-7}$ m s. The drive speed (dashed line) is -20.5 nm/s. Figure 7(a) shows the first 22 s of the response. Open circles are the experimental points; the continuous curve is the Reynolds theory. The shaded region is enlarged in Fig. 7(b), in which the curved labeled (a) is the same as in Fig. 7(a), and curve (b) is the predicted drainage for a shear plane located a distance $D_S = 1.3$ nm out from each surface. A further enlargement is shown in Fig. 7(c), in which it is seen that at small separations the drainage occurs in a series of steps of ~ 0.75 nm, which corresponds to the molecular diameter of OMCTS. Theoretical curves (a) and (b), corresponding to those in Fig. 7(b), show the same feature although the times at which the steps occur do not match the experimental results. Curve (c) is the predicted drainage for a van der Waals surface force alone, and curve (d) is for no surface force (both with $D_S = 0$).

drainage run shown in Figs. 3(a) and 3(b), in which $L(t)$ continues without limit. The results of a "standing start" run in OMCTS are shown in Fig. 7(a), together with the theoretical curve. Once again we see excellent agreement with experiment for $D \gtrsim 50$ nm, but at smaller separations the liquid film drains more slowly than the theoretical prediction.

This small but measurable discrepancy can only be accounted for by some effect which tends to increase the hydrodynamic drag

$$F_H = -\frac{6\pi\eta R_H R_G}{D}\frac{dD}{dt} \tag{4.3}$$

at small separations. One possibility is that the effective radii are increased by elastohydrodynamic flattening, but we show in Appendix C that this effect is negligible at the low speeds encountered in this experiment. Otherwise, one could postulate that η is not equal to its bulk value in very thin films, or that F_H is no longer proportional to speed and inversely proportional to distance. The first suggestion is very plausible, and indeed has been made several times before, at least for polar liquids.[9,20–24] However, in the absence of a microscopic explanation for an enhanced viscosity near a solid surface, we choose to make a much simpler suggestion: that there is an "immobile" region of liquid adjacent to each solid surface. Let this layer be of thickness D_s, so our postulate is that the stick boundary conditions apply at a distance D_s out from each surface. In this case the hydrodynamic force becomes

$$F_H = -\frac{6\pi\eta R_H R_G}{(D-2D_s)}\frac{dD}{dt} \quad (D > 2D_s). \tag{4.4}$$

This very simple-minded approach has two advantages. First, it introduces only one adjustable parameter with which to fit the experimental results, and second, it leaves the viscosity η independent of separation. If $\eta(D)$ were not a constant, it would appear inside the square bracket in Eq.

(A5), and a complete reanalysis of the hydrodynamic force would be required.

We emphasize that this is merely an empirical model which we will use in an attempt to fit the experimental data. Even if successful, we will not have *proven* that this model is physically correct, or that other models could not be equally successful (and remain equally unproven!).

The data of Fig. 7(a) for $D \leqslant 50$ nm are replotted on an enlarged scale in Fig. 7(b), to show more clearly the discrepancy between experiment and the unadulterated Reynolds theory. Incorporation of the modified hydrodynamic drag term [Eq. (4.4)] in Eq. (3.3) gives a very satisfactory fit to the experimental points for $D > 6$ nm, if we set $D_S = 1.3$ nm. At larger distances the two theoretical curves merge. Thus allowance for a very thin immobile region of liquid next to each solid surface—less than two molecular diameters thick—gives an excellent description of the experimental results as the liquid film drains right down to $D \approx 6$ nm.

In Fig. 7(c) we examine the drainage for $D \leqslant 10$ nm in more detail. The experimental data show that for $D \lesssim 5$ nm the drainage becomes irregular: the surfaces move closer in abrupt steps of ~ 0.75 nm then remain almost stationary for a period before the next step. This step size corresponds to the diameter of the OMCTS molecule, and we know that the molecules tend to be arranged in *layers* near the smooth mica surface.[11] The surfaces approach as if the liquid is being squeezed out layer by layer, although we cannot establish the exact mechanism by which this occurs.

Inclusion of an oscillatory force law (3.10) produces the same feature in the theoretical drainage curves shown in Fig. 7(c), as seen by comparing the curves labeled *a* (oscillatory surface force), *c* (van der Waals attraction only), and *d* (no surface force). The existence of a repulsion between the surfaces at certain separations (Fig. 4) does have the effect of slowing down their approach, and to this extent the stepwise drainage can be considered to be a result of the oscillatory surface force, which is itself a reflection of the layering of molecules in very thin films. However, the steps observed in the experiment occur much later than those predicted by the theory, and the inclusion of an immobile region only goes a little way towards improving this situation (curve *b*).

Clearly we are in a regime where we must consider the liquid as a collection of molecules, and continuum hydrodynamics should not be expected to remain valid. For this reason we make no attempt to seek any closer agreement between our experiment and any continuum theory. That goal must await the development of a microscopic description of the drainage of liquid films which are only a few molecular diameters thick.

The force barriers (Fig. 4) increase markedly as D decreases, and in fact prevent the surfaces from coming closer than $D \simeq 2.9$ nm in this experiment. Thus we never get the surfaces close enough to encounter the putative immobile region at $D = 2D_s = 2.6$ nm, and the restriction $D > 2D_s$ on Eq. (4.4) is never violated.

B. *n*-Tetradecane

The equilibrium force between mica surfaces in tetradecane has similar characteristics to that in OMCTS: at short range it is an oscillatory function of distance, superimposed on a monotonic van der Waals attraction.[14] The periodicity of the oscillations is only 0.40 nm, corresponding to the *width* of a linear alkane molecule. This force can be approximated by Eq. (3.10) with the parameters $A = 1.0 \times 10^{-20}$ J, $B = 49$ mN/m, and $\xi_1 = \xi_2 = 0.40$ nm.

Figure 8 shows the results of a "flying start" drainage experiment in tetradecane. Although the viscosity of this liquid, $\eta = 2.27$ cP,[25] is comparable to that of OMCTS, the radii of the mica surfaces were smaller in this experiment and so the constant $\alpha = 8.4 \times 10^{-8}$ m s was significantly smaller than for the OMCTS results presented above. As a consequence, the deflection of the spring $\Delta(t) = D(t) - L(t)$ was smaller. In Fig. 8(a) we see that the Reynolds theory (with no immobile region, $D_S = 0$) again fits the experimental results very well at large separations, but predicts too fast a drainage rate for $D \lesssim 50$ nm. This region is amplified in Fig. 8(b), and a second theoretical curve is shown: that obtained with $D_S = 0.7$ nm. Once again we find that the experimental measurements are accounted for reasonably well by simply assuming that a thin layer of liquid, less than the thickness of

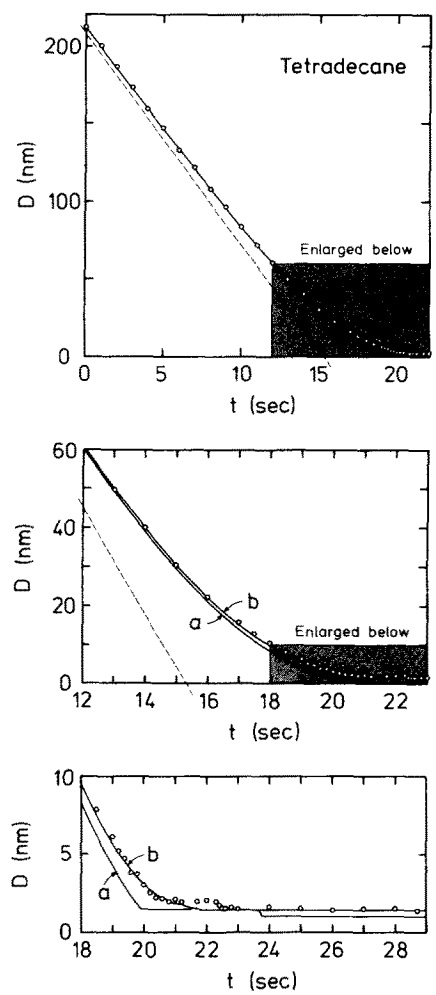

FIG. 8. Results of a flying start drainage run in *n*-tetradecane, with $\alpha = 8.4 \times 10^{-8}$ m s. Figure 8(a) shows the first 22 s, with the drive function ($V = -13.5$ nm/s) and the predicted response. The shaded region is enlarged in Fig. 8(b). Here curve (a), which corresponds to the curve shown in Fig. 8(a), is for $D_S = 0$ and curve (b) is for $D_S = 0.7$ nm. Figure 8(c) shows the drainage at small separations.

two molecules of *n*-tetradecane lying parallel to each surface, remains immobile.

Results for the drainage in very thin films, $D < 10$ nm, are reproduced in Fig. 8(c). Just as in OMCTS, we can see that the final stages of drainage occur in discrete steps, which is qualitatively but not quantitatively accounted for by including an oscillatory surface force law in the theory. The time taken to move in by one step of ~ 0.4 nm is significantly longer than the time it would take merely to push the surfaces over the repulsive force barrier at that separation: there is also some dynamic barrier (greater than expected from continuum hydrodynamics) to be overcome.

C. *n*-Hexadecane

The surface force measured in hexadecane (unpublished results) is comparable to that in tetradecane, and is approximated by Eq. (3.10) with the parameters $A = 1.0 \times 10^{-20}$ J, $B = 62$ mN/m, and $\xi_1 = \xi_2 = 0.40$ nm. The viscosity is 3.35 cP,[25] and in the experiment whose results are presented in Fig. 9, the constant α was 7.4×10^{-8} m s.

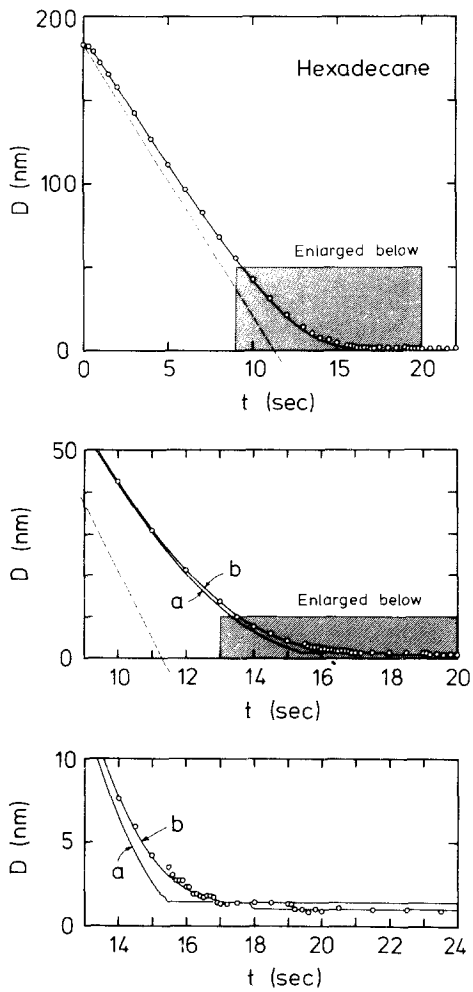

FIG. 9. A standing start drainage run in *n*-hexadecane, with $\alpha = 7.4 \times 10^{-8}$ m s and drive speed -16.2 nm/s. The continuous line in Fig. 9(a), labeled (a) in the enlargements 9(b) and 9(c), is for $D_S = 0$; curve (b) is for $D_S = 0.7$ nm. Note that at $t \approx 19$ s the hexadecane film thins to $D \approx 1.0$ nm, whereas the simple shear-plane model used to generate curve (b) would not allow the surfaces to come closer than $2D_S = 1.4$ nm.

Similar conclusions are to be drawn from the hexadecane drainage measurements. Figure 9(a) shows that the Reynolds theory works well for $D \gtrsim 50$ nm; below that [Fig. 9(b)] the inclusion of an immobile region of thickness $[SB{:}D{:}S] = 0.7$ nm accounts for the slower drainage which is measured; and stepped drainage is discernible in very thin films, $D \lesssim 2$ nm [Fig. 9(c)].

There is one noteworthy feature of the hexadecane results, which is that the surfaces come in to a separation $D \approx 1.0$ nm after 19 s. Obviously they could not do this if there really was a completely immobile layer of 0.7 nm on each surface. This experiment provides us with a salutory reminder that our model, which seems to provide a satisfactory account of the results beyond $D \sim 5$ nm, is too simple to explain what really happens in the thinnest films.

D. The effect of water in OMCTS

As mentioned in Sec. II, trace amounts of water can have a dramatic effect on the surface force measured in organic liquids.[11,12,16] Water is only slightly soluble, perhaps to a few hundred parts per million, but even at these levels it changes the picture dramatically. What matters is the chemical activity of the water, in other words the fraction of saturation, rather than the absolute amount. This is easily varied by equilibrating the liquid with an atmosphere containing water vapor at a certain activity (relative humidity or fraction of saturated vapor pressure).

As discussed by Christenson,[16] the effect of $\sim 50\%$ saturation of water in OMCTS is to reduce the outermost repulsive barriers in the oscillatory force curve (Fig. 4) so that the surfaces come more easily in to $D \sim 3$ nm before encountering any significant repulsion. As the level of water approaches 100% saturation, any force barriers closer to $D = 0$ also vanish, and the surfaces come into molecular contact. The reason for this is that water is preferentially adsorbed on the hydrophilic mica surface, and when two curved surfaces are close enough, water condenses to form a liquid bridge between them. This is accompanied by a very strong attraction between the surfaces ($F/R \sim -400$ mN/m) which pulls them into contact.[16]

The effect of this on the drainage of OMCTS films is shown in Fig. 10. At 0% water the drainage curve is similar to that shown in Fig. 7, discussed in Sec. IV A. At approximately 50% water the surfaces come in more easily to a separation of $D \approx 3$ nm, but stop there. When the OMCTS is saturated in water (250 ppm),[12] the surfaces come into contact very abruptly from $D \approx 10$ nm. This occurs in a time shorter than 0.02 s (less than one frame of the video recording).

These results clearly show the importance of the surface force in determining the drainage behavior of thin films. They also illustrate an important practical point: that the drainage of organic liquids between hydrophilic surfaces is altered radically by the presence of water. For example, a suspension of hydrophilic particles in a nonpolar liquid would flocculate very rapidly in the presence of water, leading to a high floc volume.[26]

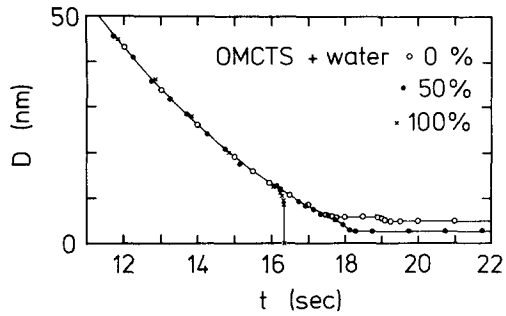

FIG. 10. The effect of trace amounts of water on the drainage of OMCTS between hydrophilic mica surfaces. Open circles show results when the atmosphere above the liquid was exposed to P_2O_5 to scavenge any water present, and are comparable to those shown in Fig. 7. The filled circles were measured with the atmosphere at approximately 50% relative humidity, and the crosses measured when it was saturated in water vapor. In the last case, the mica surfaces jump very abruptly into molecular contact from a separation of $D \approx 10$ nm (Ref. 16). (In this figure the continuous lines are drawn through the experimental points; they do not represent any theoretical predictions.)

V. DISCUSSION

The three Newtonian liquids studied here have all (when free of water) shown comparable behavior in their drainage between smooth solid surfaces, which gives us added confidence in making the following remarks.

First, from the evidence displayed in Figs. 5 and 6 and discussed in Sec. IV A, we may conclude that the liquid viscosity does not deviate measurably from its bulk value in films down to $D \sim 50$ nm thick. There have been reports of substantially increased viscosities in films of up to 100 nm thick,[9,20–24] though Derjaguin[20,22] has pointed out that these have only been observed in polar liquids. In studies of polydimethylsiloxanes (chemically similar to OMCTS) Derjaguin *et al.*[27] found no variation from the bulk viscosities down to 20 nm films, and Israelachvili[14] has found no variation in tetradecane or aqueous electrolyte solutions at any thickness. Askwith *et al.*[24] reported a constant viscosity for hexadecane in squeeze films down to 9 μm thickness, but noted that their films stopped thinning at $D \sim 2\,\mu$m, and spoke of a "plastic solid" layer at each surface, of $\sim 1\,\mu$m thick. Fuks[28] had earlier reached the same conclusion. Evidently we see nothing of that kind in the present experiment.

In thinner films, $50 \gtrsim D \gtrsim 5$ nm, the Reynolds theory continues to give an excellent description of the experimental results provided that: (i) the appropriate equilibrium force acting between the solid surfaces across the liquid in question is included in the equation of motion, and (ii) a small but distinct enhancement of the liquid viscosity is considered.

To say that there is an enhancement of viscosity in thin films implies that the viscosity of the liquid does not have its bulk value right up to the surface, in other words that it is a (nonconstant) function of distance from the solid interface. Unfortunately our experiment gives no direct information on what this function might be, because we do not measure the velocity profile within the liquid film. The best we can do is to establish an *effective* viscosity at a particular thickness of the entire film, that is to find $\eta_{\text{eff}}(D)$, with $\eta_{\text{eff}} \to \eta$, the bulk viscosity, as $D \to \infty$. In describing Figs. 7, 8, and 9 we have shown that our results are *consistent* with a model in which the liquids studied have a constant viscosity (equal to the bulk value) everywhere except in a region of thickness D_S adjacent to each solid surface. In these regions the liquid is immobile (in a sense to be discussed further below), or infinitely viscous. It turns out that the value of D_S need only correspond to a couple of molecular layers to describe our results quite accurately. Other forms of the viscosity profile, for example a well-defined thicker film of higher-than-bulk but still finite viscosity, or a viscosity which decays continuously from a high value at the surface to its bulk value, could probably be just as successful in fitting our results. However, we have chosen not to play with such models because there is no feature of our measurements, or any theoretical basis that we know of, which commends them to us.

At this stage we should note that D_S is not determined very precisely, because almost equally good fits to our data could be obtained using slightly different combinations of the driving speed V and the value of D_S in the numerical routine which generates the theoretical drainage curve. Varying V by $\sim 1\%$ (which is the experimental error in establishing this quantity when using the motor drive) can give a spread of values of D_S from about 0.8–1.5 nm for OMCTS, and from 0.5–1.0 nm for the two alkanes. Therefore we do not attach great significance to the precise value of D_S in the model we have used. We do, however, find it reassuring that D_S is a small number, only 1–2 molecular layers. It seems plausible that the flow behavior of a liquid is modified in some way by structuring of the liquid within a few molecular diameters of a solid boundary, particularly since we know from solvation force measurements that the equilibrium distribution of molecules is affected out to four or five diameters from each surface.[11] We find it more difficult to believe that any modified structure of a nonpolar liquid should extend for tens or hundreds of nanometers.

Even a very thin immobile region can have a discernible effect on the effective viscosity of a substantially thicker film. By comparing Eqs. (4.3) and (4.4), it can be seen that in our simple model

$$\eta_{\text{eff}}(D) = \frac{D}{D - 2D_S}\,\eta \tag{5.1}$$

or

$$\frac{\eta_{\text{eff}} - \eta}{\eta} = \frac{2D_S}{D - 2D_S}\,. \tag{5.2}$$

Thus the enhancement of the viscosity, which gives a good fit to our results, is 10% at $D = 29$ nm and 1% at $D = 263$ nm in OMCTS. In tetradecane and hexadecane the corresponding film thicknesses are 15 and 141 nm. Of course it is only possible for us to arrive at these estimates *because* our mica surfaces are molecularly smooth, making it possible to define (as well as measure) their separation with a precision finer than the thickness D_S. Were they rougher than this, as most surfaces are, the above discussion hinging on the difference between D and $D - 2D_S$ would depend critically on how $D = 0$ was determined. In the present experiment $D = 0$ corresponds to the mica surfaces in molecular contact in a nitrogen atmosphere. We also note that here we are determining

the effective viscosity by measuring a hydrodynamic drag force which varies as (1/distance). The difficulties would be exacerbated in measurements of quantities with stronger distance dependences, such as drainage between flat plates (fall time under constant load $\sim 1/D^2$) or flow through capillaries ($1/R^4$).

Colloid scientists and biophysicists who study electrokinetic behavior of small particles (including vesicles and cells) often tacitly make an assumption which corresponds to the model discussed here, by speaking of a "shear plane" or "slipping plane" at which the zeta potential is measured.[29] The solvent—usually water—is supposed to have a constant viscosity up to the shear plane, but the shear plane need not coincide with the surface. The consensus of opinion seems to be that the shear plane is never more than a few tenths of a nanometer from the surface (however that might be defined!),[29,30] so there would not be more than one or two layers of water molecules which do not flow according to hydrodynamic expectations.

Debye and Cleland[31] invoked a similar model to account for deviations from Poiseuille's law in their measurements of flow of *n*-alkanes through a porous glass (although they also allowed slipping at the solid boundary). They found that their results were compatible with having a thickness D_S equal to the width of a single hydrocarbon chain.

Measurements of the self-diffusion of water in polymer solutions and colloidal systems using NMR techniques suggest that there may be a couple of layers of water molecules adjacent to the polymer or colloid "surface" which do not diffuse freely.[32,33] This observation may also be related to the presence of immobile regions in shear flow next to a solid boundary.

We do not suggest that molecules of liquid are truly immobile near the solid surface. To account for the present results we need only imagine that the component of velocity *parallel* to the surface is hindered or restricted on the time scale of this experiment. The velocity normal to the surface need not be affected, and the molecules next to the surface can be exchanging rapidly with those away from it. Furthermore, we must note the evidence of Fig. 9(c), in which it is seen that after a certain time the solid surfaces in hexadecane approach to a separation less than $2D_S$, which would be impossible if these regions really were completely immobile (even in the sense described above).

In very thin films, $D \lesssim 5$ nm, the liquids drain in a series of abrupt steps each corresponding to the thickness of a molecular layer. Qualitatively, this stepwise approach of the surfaces can be understood in terms of the surface force. As the two mica sheets approach, they encounter a series of repulsive barriers of increasing height (Fig. 4) which have the effect of holding them almost stationary at certain separations, which are multiples of the molecular layer thickness.[11] Quantitatively, however, this is not the full story. The drainage of the liquid occurs even more slowly than predicted (by continuum hydrodynamics) when the surface forces are included. In other words, in films only a few molecular layers thick, the liquid does not flow as if it has a simple viscosity equal to the bulk value. This of course is no surprise: we already know that the continuum models for the surface force have broken down,[11] so the continuum description should not be expected to hold for the drainage of such thin films.

The fact that in this regime the liquid drains slower than the continuum prediction is at least consistent with the idea that resistance to shear flow *increases* within a few molecular layers of a solid surface, as assumed in the simple model of an immobile region discussed above. Perhaps the ordering of molecules into layers impedes rather than facilitates their shear. Or the proximity of the solid surfaces may prevent molecules from moving *around* each other, by restricting their motion in a direction normal to the surfaces. Whatever the correct microscopic explanation, hopefully it will not only describe the drainage in the very thinnest films, but also supplant the crude "immobile region" model used to account for the apparent enhancement in viscosity of films up to 50 nm thick, and so provide a satisfactory description of the entire drainage process.

Israelachvili[14] has recently made comparable measurements using the same apparatus, but employing an oscillatory driving function $L(t) = L_0 + A_0 e^{i\omega t}$. He studied aqueous electrolyte solutions and *n*-tetradecane, and in both cases reached the conclusions that the liquid viscosity had its bulk value even in very thin films (down to $D \approx 5$ nm) and that there was no measurable displacement of the shear plane from the surface. This is in contrast to our results, and it is not evident why we should differ on this point. The reason may lie in the fact that his measurements become less accurate for very thin films, or possibly be due to the difference in shear rates encountered in the two experiments. From Eq. (A12) we can estimate the maximum shear rate in our tetradecane experiment as 60 s^{-1} at $D = 100$ nm, 730 s^{-1} at 10 nm, 1230 s^{-1} at 5 nm, and 1830 s^{-1} at 2.5 nm. The shear rate in Israelachvili's experiment on the same liquid would have reached 200 s^{-1} at $D \approx 5$ nm. It seems surprising to us that the immobile regions should suddenly appear when the shear rate is increased by a factor of only 6.

We end this section by discussing a consequence of these observations for the measurement of surface forces using the Israelachvili apparatus. It is clear that in very thin films, the interval between "steps" inwards can become quite long, perhaps minutes [Fig. 7(c)]. This is the time scale over which our usual measurements of the surface force, supposedly equilibrium measurements, are made, and thermal drifts make it difficult in practice to increase these times. Clearly, it would be possible to make a measurement before the liquid has actually drained to its equilibrium thickness, and so the slow drainage could cause us to overestimate the force at a given distance. The difficulties due to liquid drainage will be worse in a liquid of high viscosity.[34]

VI. CONCLUSIONS

The Reynolds theory of hydrodynamic lubrication gives a very satisfactory description of the drainage of nonpolar liquids between molecularly smooth mica surfaces down to film thicknesses of ~ 50 nm. No variation of the liquid viscosity from its bulk value is measured in this regime. In thinner films there is an apparent steady enhancement of the viscosity, which is accounted for empirically by allowing the plane of shear to be about two molecular layers away from

the solid surface (towards the liquid). However, we do not claim that this simple-minded picture is a realistic model for very thin films. As the solid surfaces come closer to contact, the continuum description breaks down, and the liquid drains in a series of abrupt steps, each corresponding to a molecular layer. We suggest that the ordering of molecules of the liquid into layers next to the smooth solid surfaces *increases* their resistance to shear. A proper account of this effect would hopefully also explain the apparent enhancement of the viscosity which is measured out to $D \sim 50$ nm.

ACKNOWLEDGMENTS

We thank J. N. Israelachvili, H. K. Christenson, D. J. Evans, S. Marcelja, S. J. Miklavic, and B. W. Ninham for helpful discussions and comments on the manuscript.

APPENDIX A: THE HYDRODYNAMIC FORCE

Consider a general curved surface moving in the direction normal to a planar surface as illustrated in Fig. 11. Let the local distance between the surfaces be a prescribed function $H(x, y)$. We shall assume that the surfaces are sufficiently rigid so that any deformations of the surfaces due to surface forces and hydrodynamic stresses are negligible. A more detailed examination, given in Appendix C, shows that this assumption is justified.

When the local radii of curvature are large in comparison with the distance of closest approach between the surfaces, the flow of liquid at low Reynolds number in the region between the surfaces may be described by the lubrication approximation.[1] In this approximation it is assumed that locally, the flow is similar to that between parallel plates. That is, the lateral component of the velocity field is large and derivatives in the direction normal to the plane are dominant. In this limit, the momentum equation for the velocity field $\mathbf{v}_T$ of a viscous liquid of shear viscosity η is approximated by

$$\eta \frac{\partial^2}{\partial z^2} \mathbf{v}_T = \nabla_T P, \tag{A1}$$

where $\mathbf{v}_T = (v_x, v_y)$ and $\nabla_T = [\hat{\mathbf{x}}(\partial/\partial x), \hat{\mathbf{y}}(\partial/\partial y)]$. To leading order, the pressure P is only a function of x and y.

Using the stick boundary conditions $\mathbf{v}_T = 0$ at $z = 0$ and $z = H(x, y)$, Eq. (A1) can be integrated with respect to z to give

$$\mathbf{v}_T = \frac{1}{2\eta} z[z - H(x, y)] \nabla_T P. \tag{A2}$$

If we combine this result with the equation of continuity

$$\frac{\partial v_z}{\partial z} = -\nabla_T \cdot \mathbf{v}_T, \tag{A3}$$

together with the boundary condition $v_z = 0$ at $z = 0$, we can integrate once more with respect to z to give

$$v_z = -\frac{1}{2\eta} \nabla_T \cdot \{ [\tfrac{1}{3} z^3 - \tfrac{1}{2} z^2 H(x, y)] \nabla_T P \}. \tag{A4}$$

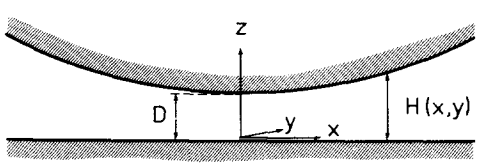

FIG. 11. Coordinate system between a curved surface and a flat plate.

At the curved surface $z = H(x, y)$, v_z is equal to the velocity of the moving surface dD/dt, hence

$$\frac{dD}{dt} = \frac{1}{12\eta} \nabla_T \cdot [H^3(x, y) \nabla_T P(x, y)]. \tag{A5}$$

This is a partial differential equation for $P(x, y)$ when the shape function $H(x, y)$ and the velocity dD/dt are prescribed.

For the geometry of two cylinders of radii R_1 and R_2 whose axes are aligned along the orthogonal y and x axes, respectively, the distance between the surfaces of the cylinders in the vicinity of the point of closest approach is given by

$$H(x, y) = D + \frac{x^2}{2R_1} + \frac{y^2}{2R_2} + O\left(\frac{1}{R_1^2}, \frac{1}{R_2^2}\right). \tag{A6}$$

For identical cylinders $R_1 = R_2 = R$, we have

$$H(x, y) = H(r) = D + \frac{r^2}{2R}, \tag{A7}$$

where $r^2 = x^2 + y^2$. For this case Eq. (A5) becomes

$$\frac{dD}{dt} = \frac{1}{12\eta} \frac{1}{r} \frac{d}{dr} \left[r H^3(r) \frac{dP(r)}{dr} \right], \tag{A8}$$

and using the condition that dP/dr is finite at $r = 0$, it may be integrated to give

$$\begin{aligned} P(r) &= P(\infty) - 6\eta \frac{dD}{dt} \int_r^\infty \frac{ds\, s}{H^3(s)} \\ &= P(\infty) - \frac{3\eta R}{H^2(r)} \frac{dD}{dt}. \end{aligned} \tag{A9}$$

Here $P(\infty)$ is the ambient pressure at $r \to \infty$. We note from Eq. (A9) that the pressure is only a function of position via the function $H(r)$, i.e., $P(r) = P(H(r))$.

Putting Eqs. (A9) and (A7) into Eq. (A2) enables us to calculate the shear rate

$$\frac{\partial v_T(r,z)}{\partial z} = -\frac{3r}{H^3(r)} [2z - H(r)] \frac{dD}{dt}. \tag{A10}$$

The shear rate is greatest at each surface, $z = 0$ and $z = H(r)$, where

$$\left| \frac{\partial v_T(r, z = 0, H)}{\partial z} \right| = \frac{3r}{(D + r^2/2R)^2} \frac{dD}{dt}. \tag{A11}$$

This has its maximum value at $r = (2RD/3)^{1/2}$, at which

$$\left| \frac{\partial v_T}{\partial z} \right|_{\max} = \frac{1}{2} \left(\frac{3}{2} \right)^{5/2} \frac{R^{1/2}}{D^{3/2}} \frac{dD}{dt}. \tag{A12}$$

For nonidentical cylinders ($R_1 \neq R_2$) Eq. (A5) reads

$$\begin{aligned} \frac{dD}{dt} = \frac{1}{12\eta} \left\{ \frac{\partial}{\partial x} \left[H^3(x, y) \frac{\partial P(x, y)}{\partial x} \right] \right. \\ \left. + \frac{\partial}{\partial y} \left[H^3(x, y) \frac{\partial P(x, y)}{\partial y} \right] \right\}. \end{aligned} \tag{A13}$$

As with the case of identical cylinders, we seek a solution of the form $P(x, y) = P(H(x, y))$, and assume the ansatz[35] [see Eq. (A9)]

$$P(x, y) = P(H(x, y)) = P(\infty) - \frac{3\eta R_H}{H^2(x, y)} \frac{dD}{dt} \tag{A14}$$

with R_H being a constant to be determined. Combining Eqs. (A6), (A13), and (A14) we find R_H to be the harmonic mean of R_1 and R_2,

$$\frac{1}{R_H} = \frac{1}{2}\left(\frac{1}{R_1} + \frac{1}{R_2}\right). \tag{A15}$$

Since the solution given by Eqs. (A14) and (A15) obeys the differential equation (A13) and all the boundary conditions, it is the unique solution for Reynolds flow between a plane and a general curved surface characterized by local principal radii of curvature R_1 and R_2.

The hydrodynamic force F_H in the normal direction between the surfaces due to viscous dissipation may be obtained by integrating the total stress on the plane surface[36]

$$F_H = \int_{-\infty}^{\infty} dx \int_{-\infty}^{\infty} dy \left[P(x,y) - P(\infty) - 2\eta \frac{\partial v_z}{\partial z}\right]_{z=0}$$
$$= -6\pi\eta R_H R_G \frac{1}{D}\frac{dD}{dt}, \tag{A16}$$

where $R_G = (R_1 R_2)^{1/2}$ is the geometric mean.

APPENDIX B: SOLUTION TO THE EQUATION OF MOTION IN THE ABSENCE OF SURFACE FORCES

As discussed in the text (Sec. III), surface forces can be neglected for $D \gtrsim 20$ nm. The equation of motion (3.3) can then be analyzed for the various types of driving function illustrated in Fig. 3, as follows.

1. Surfaces driven together with "flying start"

In this situation [Fig. 3(a)] the surfaces have been set in motion at some earlier time $t < 0$. The driving function is

$$L(t) = D(0) - \Delta(0) + Vt, \tag{B1}$$

where $V < 0$ and

$$\Delta(0) = -\frac{\alpha}{D(0)}\frac{dD}{dt}\Big|_{t=0}, \tag{B2}$$

in which we have set

$$\alpha = \frac{6\pi\eta R_H R_G}{K}. \tag{B3}$$

This parameter, with dimensions $[LT]$, incorporates all of the quantities which remain fixed in a particular experiment. Equation (3.3), together with Eq. (3.5) and (3.7) becomes

$$\frac{\alpha}{D(t)}\frac{dD(t)}{dt} = D(0) - D(t) - \Delta(0) + Vt. \tag{B4}$$

We change to the new dependent variable

$$y(x) = \frac{D(0)}{D(t)}, \tag{B5}$$

where

$$x = \frac{D(0)}{\alpha}t, \tag{B6}$$

and introduce the dimensionless constants

$$\gamma = \frac{-6\pi\eta R_H R_G}{K}\frac{V}{D^2(0)} = -\frac{\alpha V}{D^2(0)} \tag{B7}$$

and

$$\delta = \frac{\Delta(0)}{D(0)} = -\frac{\alpha}{D^2(0)}\frac{dD}{dt}\Big|_{t=0}. \tag{B8}$$

Note that both γ and δ are positive, since $V < 0$ and $dD/dt < 0$ when the surfaces are being driven together. Equation (B4) then becomes the linear differential equation

$$\frac{dy(x)}{dx} = 1 + [\gamma x + \delta - 1]\, y(x), \tag{B9}$$

whose solution is

$$y(x) = e^{-(1-\delta)x + \gamma x^2/2}\left[1 + \int_0^x e^{(1-\delta)s - \gamma s^2/2}\, ds\right]. \tag{B10}$$

This can be rewritten as

$$y(x) = e^{\xi^2 - [(1-\delta)^2/2\gamma]}\left\{1 + \left(\frac{\pi}{2\gamma}\right)^{1/2} e^{[(1-\delta)^2/2\gamma]} \times\left[\operatorname{erf}\left(\frac{1-\delta}{(2\gamma)^{1/2}}\right) + \operatorname{erf}(\xi)\right]\right\}, \tag{B11}$$

where

$$\xi = \left(\frac{\gamma}{2}\right)^{1/2} x - \frac{(1-\delta)}{(2\gamma)^{1/2}} = \left(\frac{-V}{2\alpha}\right)^{1/2}(t - t^*) \tag{B12}$$

and

$$t^* = \frac{D(0) - \Delta(0)}{-V} = \frac{L(0)}{-V} \tag{B13}$$

is the time at which $L(t) = 0$ [see Fig. 3(a)]. The error function appearing in Eq. (B11) is

$$\operatorname{erf}(z) = \frac{2}{\sqrt{\pi}}\int_0^z e^{-x^2}\, dx$$

and we have used the identity $\operatorname{erf}(-z) = -\operatorname{erf}(z)$.

2. Surfaces driven together, with "standing start"

If the surfaces are at rest before the driving function is switched on at $t = 0$, we see from Eq. (B2) that

$$\Delta(0) = 0 \tag{B14}$$

and from Eq. (B1),

$$L(t) = D(0) + Vt \tag{B15}$$

with $V < 0$ [see Fig. 3(b)]. The analysis of the previous section carries over, with [from Eq. (B8)] $\delta = 0$ in the results (B10)–(B12).

3. Surfaces driven together for a limited time

Another possible driving function is illustrated in Fig. 3(c), in which the remote end of the spring is driven inwards ($V < 0$) during the interval $0 \leqslant t \leqslant t_s$, and is held stationary for $t < 0$ and $t > t_s$. Thus $L(t)$ has the form

$$L(t) = D(0) + Vt, \quad 0 \leqslant t \leqslant t_s, \tag{B16a}$$
$$= D(0) + Vt_s = L_\infty, \quad t \geqslant t_s. \tag{B16b}$$

The equation of motion (B9) becomes

$$\frac{dy}{dx} = 1 - [1 - \gamma x]\, y, \quad 0 \leqslant x \leqslant x_s, \tag{B17a}$$
$$= 1 - [1 - \gamma x_s]\, y, \quad x \geqslant x_s, \tag{B17b}$$

where

$$x_s = \frac{D(0)}{\alpha}t_s. \tag{B18}$$

The solution is [cf. Eq. (B10)]

$$y(x) = e^{-x+\gamma x^2/2}\left[1 + \int_0^x e^{s-\gamma s^2/2}\,ds\right], \quad 0 \leqslant x \leqslant x_s, \tag{B19a}$$

$$= e^{-\lambda x}\left|y(x_s)e^{\lambda x} + (1/\lambda)(e^{\lambda x} - e^{\lambda x_s})\right|, \quad x \geqslant x_s, \tag{B19b}$$

where

$$\lambda = 1 - \gamma x_s = 1 + \left[\frac{\alpha V}{D^2(0)}\right]\left[\frac{D(0)}{\alpha}\,t_s\right] = \frac{L_\infty}{D(0)}. \tag{B20}$$

Let us examine the solution for $x \geqslant x_s$, i.e., after the drive is switched off; this will be found useful in Sec. IV. After rearranging Eq. (B19b) we find (for $L_\infty \neq 0$)

$$y(x) - \frac{1}{\lambda} = \left(y(x_s) - \frac{1}{\lambda}\right)e^{-\lambda(x-x_s)}. \tag{B21}$$

Substituting from Eqs. (B5), (B6), (B18), and (B20) gives

$$\frac{D(t) - L_\infty}{D(t)} = \frac{D(t_s) - L_\infty}{D(t_s)}\,e^{-(L_\infty/\alpha)(t-t_s)}. \tag{B22}$$

Thus, for $L_\infty > 0$, the quantity $[D(t) - L_\infty]/D(t)$ decreases exponentially towards zero with the decay time α/L_∞. The analysis is still valid for $L_\infty < 0$, but now the solution grows indefinitely, i.e., $D(t) \to 0$ as $t \to \infty$.

To solve the special case $L_\infty = 0$, we go back to the original equation (B17b) and put $1 - \gamma x_s = 0$, so

$$dy/dx = 1. \tag{B23}$$

The solution is

$$y(x) = y(x_s) + x - x_s \tag{B24}$$

or

$$\frac{1}{D(t)} = \frac{1}{D(t_s)} + \frac{t - t_s}{\alpha}. \tag{B25}$$

4. Pulling surfaces apart for limited time

Figure 3(d) illustrates the case in which the surfaces are pulled apart during the time interval $0 \leqslant t \leqslant t_s$. We have

$$L(t) = D(0) + Vt, \quad 0 \leqslant t \leqslant t_s, \tag{B26a}$$

$$= D(0) + Vt_s = L_\infty, \quad t \geqslant t_s \tag{B26b}$$

with $V > 0$. From Eq. (B7) we now have $\gamma < 0$. Writing

$$\beta = \left(\frac{-\gamma}{2}\right)^{1/2} = \frac{1}{D(0)}\left(\frac{\alpha V}{2}\right)^{1/2} \tag{B27}$$

the solution to Eq. (B26a) can be expressed as

$$y(x) = e^{-x-\beta^2 x^2}\left[1 - \frac{1}{\beta}F\left(\frac{1}{2\beta}\right)\right] + \frac{1}{\beta}F\left(\beta x + \frac{1}{2\beta}\right), \quad 0 \leqslant x \leqslant x_s, \tag{B28}$$

where

$$F(z) = e^{-z^2}\int_0^z e^{s^2}\,ds \tag{B29}$$

is Dawson's integral.

The solution to Eq. (B26b) follows that of the previous section. Since $\gamma < 0$ in Eq. (B20), L_∞ is always positive, and we have [from Eq. (B22)]

$$\frac{L_\infty - D(t)}{D(t)} = \frac{L_\infty - D(t_s)}{D(t_s)}\,e^{-(L_\infty/\alpha)(t-t_s)}, \quad t \geqslant t_s. \tag{B30}$$

APPENDIX C: ELASTOHYDRODYNAMIC FLATTENING

If the solid surfaces are not perfectly rigid, they can be deformed by a nonuniform distribution of pressure between them. Such nonuniform pressure can arise from two sources: hydrodynamic pressure and surface forces. The first effect is called elastohydrodynamic deformation, and has been extensively studied in the lubrication literature[2,37]; the second has been called the soft-contact problem, and studied by Hughes and White.[38] Both are very difficult to solve exactly, because a nonuniform pressure distribution causes a deformation which changes the surface profile, which in turn modifies the original pressure distribution. To write a solution in closed form requires integral equations, which can generally only be solved numerically for a particular case.

No attempt has been made to compute the surface deformation in the presence of an oscillatory solvation force. We have observed experimentally[11,12] that perceptible flattening of the surfaces occur under large repulsive forces, typically for $F/R \gtrsim 1$ mN/m, which occurs at $D \approx 3$–4 nm in the OMCTS experiment reported here. This effect causes us to overestimate the true value of F/R in the neighborhood of repulsive maxima, because we still divide the measured load F by the *undistorted* radius R.

To estimate the importance of elastohydrodynamic flattening in the present experiment, we do not solve the problem completely, but calculate the amount by which the central part of the surface, i.e., at the point of closest approach, would be displaced elastically by the hydrodynamic pressure distribution Eq. (A9). This is given by

$$\delta D = \frac{2(1-\sigma^2)}{E}\int_0^\infty [P(r) - P(\infty)]\,dr, \tag{C1}$$

where σ is Poisson's ratio and E is Young's modulus of the solids. Putting

$$P(r) - P(\infty) = -\frac{3\eta R}{(D + r^2/2R)^2}\frac{dD}{dt} \tag{C2}$$

in this expression leads to the result

$$\delta D = -\frac{3\pi\eta}{4}\left(\frac{1-\sigma^2}{E}\right)\left(\frac{2R}{D}\right)^{3/2}\frac{dD}{dt}. \tag{C3}$$

(This result was quoted incorrectly in Ref. 11, by a factor $2^{5/2}$.)

For our experimental system, $E/(1-\sigma^2)$ is estimated as 10^{10} N/m^2.[39,40] Using other data appropriate to the OMCTS experiment shown in Fig. 7, we find this first-order estimate of the central displacement gives $\delta D = 0.007$ nm at $D = 50$ nm, and 0.05 nm at $D = 5$ nm. We conclude that elastohydrodynamic flattening can safely be ignored in this system.

[1] O. Reynolds, Philos. Trans. R. Soc. London **177**, 157 (1886).
[2] See for example O. Pinkus and B. Sternlicht, *Theory of Hydrodynamic Lubrication* (McGraw-Hill, New York, 1961); A. Cameron, *The Principles of Lubrication* (Longmans, London, 1966).
[3] I. B. Ivanov and R. K. Jain, in *Dynamics and Instability of Fluid Interfaces*, edited by T. S. Sorenson (Springer, Berlin, 1979), p. 120.
[4] I. B. Ivanov, Pure Appl. Chem. **52**, 1241 (1980).
[5] D. S. Dimitrov, Prog. Surf. Sci. **14**, 295 (1983).

[6]J. A. Kitchener, in *Recent Progress in Surface Science*, edited by J. F. Danielli, K. G. A. Pankhurst, and A. C. Riddiford (Academic, New York, 1964), Vol. 1, p. 51.
[7]A. Scheludko, Adv. Colloid Interface Sci. **1**, 391 (1967).
[8]R. Buscall and R. H. Ottewill, in *Colloid Science*, edited by D. H. Everett (The Chemical Society, London, 1975), Vol. 2, p. 191.
[9]D. B. Hough and R. H. Ottewill, Prog. Colloid Polym. Sci. **68**, 101 (1983).
[10]J. N. Israelachvili and G. E. Adams, J. Chem. Soc. Faraday Trans. 1 **74**, 975 (1978).
[11]R. G. Horn and J. N. Israelachvili, J. Chem. Phys. **75**, 1400 (1981).
[12]H. K. Christenson, J. Chem. Phys. **78**, 6906 (1983).
[13]R. M. Pashley and J. N. Israelachvili, J. Colloid Interface Sci. **101**, 511 (1984).
[14]J. N. Israelachvili, J. Colloid Interface Sci. (in press).
[15]S. Tolansky, *Multiple-beam Interferometry of Surfaces and Films* (Clarendon, Oxford, 1948).
[16]H. K. Christenson, J. Colloid Interface Sci. **104**, 234 (1985).
[17]B. V. Derjaguin, Kolloid Zh. **69**, 155 (1934). For a more recent derivation of the Derjaguin approximation, see L. R. White, J. Colloid Interface Sci. **95**, 286 (1983).
[18]H. K. Christenson and J. N. Israelachvili, J. Chem. Phys. **80**, 4566 (1984).
[19]K. N. Marsh, Trans. Faraday Soc. **64**, 1 (1968).
[20]B. V. Derjaguin, Chem. Scr. **9**, 97 (1976).
[21]Z. M. Zorin, V. D. Sobolev, and N. V. Churaev, in *Research in Surface Forces*, edited by B. V. Deryagin (*sic*) (Consultants Bureau, New York, 1975), Vol. 4, p. 232.
[22]B. V. Derjaguin, Yu. M. Popovskij, and B. A. Altoiz, J. Colloid Interface Sci. **96**, 492 (1983).
[23]W. Drost-Hansen, in *Biophysics of Water*, edited by F. Franks and S. Mathias (Wiley, New York, 1982), p. 163.
[24]T. C. Askwith, A. Cameron, and R. F. Crouch, Proc. R. Soc. London Ser. A **291**, 500 (1966).
[25]F. D. Rossini, K. S. Pitzer, R. L. Arnett, R. M. Braun, and G. C. Pimental, *Selected Values of Physical and Thermodynamic Properties of Hydrocarbons and Related Compounds* (Carnegie, Pittsburgh, 1953).
[26]C. R. Bloomquist and R. S. Shutt, Ind. Eng. Chem. **32**, 327 (1940).
[27]B. V. Deryagin (*sic*), V. V. Karasev, I. A. Lavygin, I. I. Skorokhodov, and E. N. Khromova, in *Research in Surface Forces*, edited by B. V. Deryagin (*sic*) (Consultants Bureau, New York, 1975), Vol. 4, p. 227.
[28]G. I. Fuks, in *Research in Surface Forces*, edited by B. V. Deryagin (*sic*) (Consultants Bureau, New York, 1962), Vol. 1, p. 79.
[29]R. J. Hunter, *Zeta Potential in Colloid Science* (Academic, London, 1981).
[30]A. Mpandou and B. Siffert, J. Colloid Interface Sci. **102**, 138 (1984).
[31]P. Debye and R. L. Cleland, J. Appl. Phys. **30**, 843 (1959).
[32]L. Piculell, Thesis, Department of Physical Chemistry 1, University of Lund, Sweden.
[33]F. D. Blum (private communication).
[34]H. K. Christenson and R. G. Horn, J. Colloid Interface Sci. **103**, 50 (1985).
[35]P. L. Kapitsa, Zh. Tekh. Fiz. **25**, 747 (1955). [Cited in Cameron, Ref. 2(b), p. 181.]
[36]L. D. Landau and E. M. Lifshitz, *Fluid Mechanics* (Pergamon, Oxford, 1959), p. 50.
[37]D. F. Moore, *The Friction and Lubrication of Elastomers* (Pergamon, Oxford, 1972).
[38]B. D. Hughes and L. R. White, Q. J. Mech. Appl. Math. **32**, 445 (1979).
[39]B. D. Hughes and L. R. White, J. Chem. Soc. Faraday Trans. 1 **76**, 963 (1980).
[40]R. G. Horn, J. N. Israelachvili, and F. Pribac (in preparation).